MOLECULAR AND CELLULAR BIOLOGY, June 2008, p. 3700–3712 Vol. 28, No. 11
0270-7306/08/$08.00+0 doi:10.1128/MCB.02038-07

Evidence for a Superoxide Permeability Pathway in Endosomal Membranes[▽]

Davis R. Mumbengegwi,[1] Qiang Li,[1] Canhui Li,[3] Christine E. Bear,[3] and John F. Engelhardt[1,2]*

Department of Anatomy and Cell Biology[1] and Center for Gene Therapy,[2] College of Medicine, University of Iowa, Iowa City, Iowa 52242, and Programme in Molecular Structure and Function, Research Institute, Hospital for Sick Children, Toronto, Ontario MG5 1X8, Canada[3]

Received 12 November 2007/Returned for modification 4 January 2008/Accepted 24 March 2008

The compartmentalized production of superoxide ($\cdot O_2^-$) by endosomal NADPH oxidase is important in the redox-dependent activation of NF-κB following interleukin 1β (IL-1β) stimulation. It remains unclear how $\cdot O_2^-$ produced within endosomes facilitates redox-dependent signaling events in the cytoplasm. We evaluated $\cdot O_2^-$ movement out of IL-1β-stimulated endosomes and whether SOD1 at the endosomal surface mediates redox-signaling events required for NF-κB activation. The relative outward permeability of NADPH-dependent $\cdot O_2^-$ from fractionated endosomes was assessed using membrane-permeable (luminol and lucigenin) and -impermeable (isoluminol) luminescent probes for $\cdot O_2^-$. In these studies, ~60% of $\cdot O_2^-$ efflux out of endosomes was inhibited by treatment with either of two anion channel blockers, 4′-diisothiocyano-2,2′-disulfonic acid stilbene (DIDS) or niflumic acid (NFA). Furthermore, radioisotopic electrodiffusion flux assays on endomembrane proteoliposomes suggested that $\cdot O_2^-$ and Cl^- are transported through the same DIDS-sensitive channel(s). Rab5-based immunoaffinity isolation of IL-1β-stimulated early endosomes demonstrated SOD1 recruitment to endosomes harboring the IL-1 receptor. Finally, SOD1-deficient cells were found to be defective in their ability to activate NF-κB following IL-1β stimulation. Together, these results suggest that $\cdot O_2^-$ exits endosomes through a DIDS-sensitive chloride channel(s) and that SOD1-mediated dismutation of $\cdot O_2^-$ at the endosomal surface may produce the localized H_2O_2 required for redox-activation of NF-κB.

The production of reactive oxygen species (ROS), including $\cdot O_2^-$ and H_2O_2, by the NADPH oxidase (Nox) complex has been implicated in signal transduction following receptor stimulation by ligands such as tumor necrosis factor, interleukin 1 (IL-1), AngII, and platelet-derived growth factor (PDGF) (28, 31). NADPH oxidases are membrane-bound, multisubunit enzyme complexes that produce $\cdot O_2^-$ by catalyzing the transfer of an electron from NADPH to oxygen (14, 18). Seven NADPH oxidase catalytic subunits are known to exist: Nox1, Nox2^{gp91phox}, Nox3, Nox4, Nox5, Duox1, and Duox2 (14, 18). Of these, the best-studied is the phagocytic gp91phox (Nox2), which is also expressed at lower levels in nonphagocytic cell types (19, 20, 27, 32). It is generally accepted that Nox complexes produce $\cdot O_2^-$ on the extracytoplasmic face of cellular membranes (31). In the context of plasma membrane-bound Nox complexes, this would produce $\cdot O_2^-$ outside the cell. In contrast, intracellular Nox complexes produce $\cdot O_2^-$ in the lumen of a vesicular compartment (20).

Links between Nox activation and redox-dependent cellular signaling have become increasingly recognized, and the localized production of $\cdot O_2^-$ appears to be a major regulatory aspect of pathways that depend on Nox-derived ROS (31). Although ROS are well known to play important roles in various signal transduction pathways that are activated in response to environmental factors, the fundamental mechanisms that link the activation of ROS production to functionally significant changes in downstream signaling cascades remain only superficially characterized. Despite this general gap in our knowledge, one concrete example of the consequences of ROS action in cell signaling exists—the inhibition of protein phosphatases by H_2O_2 (28, 29). Such a mechanism is used in the inactivation of a JNK phosphatase crucial to TNF-mediated apoptosis (17). Similarly, peroxiredoxin II has been shown to negatively regulate PDGF signaling by controlling the activity of protein tyrosine phosphatases that are important in the inactivation of the PDGF receptor (4). A second mechanism whereby H_2O_2 can signal is by altering protein structure, for example through the oxidation of reactive thiols (8). As shown recently, IL-1β-induced ROS production by Nox2 in the endosomal compartment is required for the localized redox-dependent recruitment of TRAF6 to ligand-activated IL-1 receptor through a mechanism thought to involve redox modification of reactive cysteines (20).

Given the importance of membrane topology in Nox-mediated ROS production and downstream redox signaling (31), a better understanding of where $\cdot O_2^-$ is converted to H_2O_2 is critical. $\cdot O_2^-$ dismutation to H_2O_2 is likely required for many redox-signaling events, and although it can occur spontaneously, it is rapidly accelerated (more than 1,000-fold) by any of the three isoforms of the superoxide dismutase enzyme (SOD1, -2, and -3). SOD1 is the cytosolic isoform (5) and was recently shown to be actively recruited to redox-active endosomes following IL-1 stimulation (20). Although the functions of SOD1 in cell signaling remain obscure, its recruitment to endosomes suggests the possibility that $\cdot O_2^-$ is actively converted to H_2O_2 on the endosome surface to facilitate localized redox-signaling events. In support of this hypothesis, it was recently demonstrated that SOD1 can regulate endosomal

* Corresponding author. Mailing address: Room 1-111 BSB, Department of Anatomy and Cell Biology, College of Medicine, University of Iowa, 51 Newton Road, Iowa City, IA 52242. Phone: (319) 335-7744. Fax: (319) 335-6581. E-mail: john-engelhardt@uiowa.edu.

▽ Published ahead of print on 31 March 2008.

Nox2 activity by binding to Rac1 (a coactivator of Nox2) and regulating Rac1-GTPase activity in a redox-dependent fashion (12). In this context, $\cdot O_2^-$ can uncouple SOD1 binding from Rac1, leading to enhanced conversion of Rac1-GTP to Rac1-GDP, resulting in Nox complex inactivation. These new findings place SOD1 central to redox-dependent regulation of Nox activity at the level of the endosome. However, it is currently unknown how $\cdot O_2^-$ might exit endosomes and act as a substrate for SOD1 in this regulatory process. Unlike with H_2O_2, which freely diffuses across membranes (3), cellular membranes are relatively impermeable by $\cdot O_2^-$ (22, 30) due to the fact that it is weakly basic and highly soluble in water at physiological pH. However, $\cdot O_2^-$ can be protonated to hydroperoxyl radicals at low pH ($pK_a = 4.8$), and the uncharged form of the molecule is membrane permeable.

The limited membrane permeability of $\cdot O_2^-$ at neutral pHs appears to enable mitochondria to control $\cdot O_2^-$ release into the cytoplasm (2). In this context, a 4,4′-diisothiocyano-2,2′-disulfonic acid stilbene (DIDS)-sensitive voltage-dependent anion channel appears to regulate the transport of $\cdot O_2^-$ anions across the outer mitochondrial membrane (11). The involvement of a similar anion channel in $\cdot O_2^-$ transport has also been observed in erythrocyte ghost membranes (22, 23) and amniotic cells (16). Recently, a DIDS-sensitive $\cdot O_2^-$ flux across the plasma membrane of endothelial cells was suggested to occur through chloride channel 3 (ClC-3) (13). This pathway of $\cdot O_2^-$ influx into endothelial cells has been shown to induce intracellular calcium release and the downstream stimulation of mitochondrial $\cdot O_2^-$ production.

Despite the increasing evidence for the existence of $\cdot O_2^-$ channels, little is known about $\cdot O_2^-$ permeability across intracellular vesicles and whether this might be important in cell signaling by Nox complexes. We hypothesized that the intravesicular $\cdot O_2^-$ that is generated following IL-1 stimulation might also utilize anion channels to cross endosomal membranes. Such a finding would help to explain why SOD1 is recruited to IL-1-stimulated Nox-active endosomes—to facilitate the local production of H_2O_2 at the endosomal surface. To test this hypothesis, we have evaluated IL-1-stimulated NADPH-dependent production of $\cdot O_2^-$ and the permeability of this anion in intact isolated endosomes, using anion channel blockers and $\cdot O_2^-$ probes with selective membrane permeability. Additionally, using reconstituted endosomal proteoliposomes loaded with xanthine-xanthine oxidase (X/XO), we investigated whether Cl^- and $\cdot O_2^-$ are transported through similar anion channels in endosomal membranes. Our results demonstrate that Nox-active endosomes indeed contain anion channels capable of facilitating the movement of $\cdot O_2^-$ across membranes. Furthermore, our data show that SOD1 is actively recruited to vesicles harboring ligand-activated IL-1 receptors and that in the absence of SOD1, NF-κB activation is impaired. These findings support the notion that $\cdot O_2^-$ may be converted to H_2O_2 at the endosomal surface and that this process is important for redox signaling.

MATERIALS AND METHODS

Cytokine treatments and isolation of intact endosomes and endomembranes. MCF-7 cells (of mammary epithelial tumor cell origin) were treated with 5 ng/ml recombinant human IL-1β (Sigma-Aldrich) or an equivalent amount of vehicle for 20 min at 37°C. The cells were then harvested, washed three times with ice-cold phosphate-buffered saline (PBS), and collected by scraping and centrifugation. The final cell pellet was resuspended in cold homogenization buffer (0.25 M sucrose, 10 mM HEPES with an EDTA-free protease inhibitor cocktail tablet; Roche) and homogenized by nitrogen cavitation at 750 lb/in^2 for 5 min. The cell lysate was then centrifuged at 1,500 × *g* at 4°C for 15 min. The postnuclear supernatant (PNS) was subsequently combined with 60% iodixanol (OptiPrep Axis-Shield) solution to produce a final concentration of 32% and was bottom loaded under two-step gradients of 24% and 20% iodixanol in homogenization buffer in an sw55Ti centrifuge tube. The samples were then centrifuged at 30,500 rpm for 2 h at 4°C. Fractions were collected from the top to the bottom of the centrifuge tube at 4°C (500 μl per fraction) and utilized immediately for the NADPH-dependent $\cdot O_2^-$ assays. Endomembranes used for generating proteoliposomes were collected from pooled endosome fractions showing peak Nox activity after iodixanol fractionation and concentrated by centrifugation at 100,000 × *g* for 2 h. The endomembrane pellet was then resuspended in homogenization buffer and stored at −80°C.

NADPH-dependent $\cdot O_2^-$ assays on isolated endosomes. NADPH oxidase activities were analyzed by measuring the relative rate of $\cdot O_2^-$ generation using chemiluminescence as detected by lucigenin (Sigma-Aldrich), luminol, or isoluminol (Fluka). Isolated endosomes were incubated in the dark with lucigenin (5 μM), luminol, or isoluminol (50 μM) for 10 min, and NADPH oxidase activity was initiated by the addition of 100 μM of NADPH (Sigma-Aldrich). The rate of light production within the first 5 min was used as a relative index of $\cdot O_2^-$ production, as previously described (20). For quenching studies, SOD1 (0.01 mg/ml) was added to the endosomes prior to addition of NADPH. In channel inhibition studies, the endosomes were incubated with 100 μM DIDS or niflumic acid (NFA) and lucigenin, luminol, or isoluminol prior to the addition of NADPH. For endosomal loading experiments, MCF-7 cells were incubated with 1 mg/ml of purified bovine SOD1 (Oxis Research) for 15 min prior to IL-1β treatment and endosomal fractionation. Subcellular fractions were then assayed for $\cdot O_2^-$ production and evaluated by Western blotting for the uptake of SOD1 and the abundance of Rab11 (a general control for endosomal loading).

Ultrastructural localization of IL-1R1 and SOD1 on isolated Rab5-expressing endosomes. Rab5-expressing early endosomes were isolated as previously described, from MCF-7 cells infected with a recombinant adenovirus expressing hemagglutinin (HA)-tagged Rab5 (20). In brief, this procedure used iodixanol-fractionated endosomes for immunoaffinity isolation by Dynabeads M-500 (Dynal Bioscience) that were coated with the anti-HA antibody. Following immunoisolation of HA-Rab5-expressing endosomes, Dynabeads with bound vesicles were fixed with 2% paraformaldehyde for 20 min at room temperature and then with 0.05 M glycine for 15 min. The Dynabeads were then transferred to an Aurion blocking buffer for 45 min. After being washed, the Dynabeads were incubated with primary antibodies (mouse anti-Cu/ZnSOD and rabbit anti-IL-1 receptor 1 [IL-1R1]) overnight at 4°C and then with gold-conjugated anti-mouse (0.8-nm gold particles) and anti-rabbit (12-nm gold particles) antibodies for 2 h. After being washed with a blocking buffer and then with PBS, the Dynabeads were postfixed in 2% glutaraldehyde for 10 min, washed again with PBS, and finally washed with water. Beads were embedded in Epon resin and sectioned (80 nm) for analysis by transmission electron microscopy (TEM). Gold was enhanced with Ag^+ for 10 to 15 min to facilitate the detection of 0.8-nm gold particles.

Subcellular localization of redox-active endosomes. Cellular localization of endosomal $\cdot O_2^-$ was performed as recently described for MCF-7 cells (20, 26), using an Oxyburst green-bovine serum albumin (BSA) conjugate loaded into the endosomal compartment. H_2HFF (Oxyburst green; Molecular Probes)-BSA stock solutions (1 mg/ml) were generated immediately prior to use by dissolving H_2HFF-BSA in deoxygenated PBS, under argon and protected from light. Cells were incubated in the presence of 50 μg/ml Oxyburst green-BSA for 2 min at 37°C and then stimulated by the addition of IL-1β (50 ng/ml). For DIDS inhibition experiments, 500 μM DIDS was added 10 min prior to IL-1β stimulation. The cells were fixed in 4% paraformaldehyde for 10 min and stained in mounting medium with 4′,6′-diamidino-2-phenylindole (DAPI) and antifadent (Vectashield; Vector Laboratories) before they were evaluated using a spinning-disk fluorescent microscope. The average H_2HFF signal per cell was quantified blindly (using NIH ImageJ software) from 20 63× fields for each condition. Cells were costained with DAPI for accurate quantification of cells. The relative fluorescent units per cell were then calculated from at least three independent cultures of MCF-7 cells.

Electrogenic flux assays. Liposomes for electrogenic flux assays were prepared as follows. Phospholipids were dissolved in chloroform, at a phosphatidylethanolamine-phosphatidylserine-phosphatidylcholine (all from Avanti Polar Lipids Inc.)-ergosterol (Sigma-Aldrich) ratio of 5:2:1:1 (mg). The chloroform was evaporated using a nitrogen gas stream, leaving an even layer of lipids on the bottom

of a round-bottomed flask. The lipid film was freeze-dried for at least 2 h to remove all solvent, after which it was hydrated with 150 mM KCl to a final lipid/liposome concentration of 10 mg/ml. The liposome mixture was then freeze-thawed three times in liquid nitrogen, after which endomembranes were added to produce a concentration of 2.5 μg protein/mg lipid. The proteoliposomes were freeze-thawed again and then sonicated until the solution became translucent. The proteoliposomes were then eluted down a Sephadex G-50 column equilibrated with glutamate buffer (125 mM potassium glutamate, 25 mM sodium glutamate, 10 mM glutamic acid, 20 mM Tris-glutamate [pH 7.6]) to remove Cl^- from the external solution. The uptake of radioactive Cl^- was initiated by the addition of 1.4 μl of ^{36}Cl (1.0 μCi/mol) to 500 μl of proteoliposome suspension and incubated for 20 min at room temperature. The accumulation of intravesicular ^{36}Cl was assayed by scintillation counting after the proteoliposomes were passed through a Dowex-1 ion-exchange column to remove extravesicular Cl^- anions. To evaluate whether $\cdot O_2^-$ flux occurred through chloride permeability pathways, we tested whether $\cdot O_2^-$ could dissipate the driving force for ^{36}Cl flux into proteoliposomes by adding xanthine (100 μM) and xanthine oxidase (0.02 U) at the same time as ^{36}Cl. Proteoliposomes were then incubated for 20 min prior to elution over the Dowex-1 column. In control experiments, $\cdot O_2^-$ was removed following a 20-min exposure to X/XO (by the addition of purified bovine SOD1 to a final concentration of 0.01 mg/ml for 10 min) prior to assessing ^{36}Cl uptake into proteoliposomes for 20 min. To investigate whether DIDS could inhibit ^{36}Cl flux, 100 μM DIDS was added to proteoliposomes. This was done during freeze-thawing, which allowed both faces of the lipid membrane to be exposed to the inhibitor; this approach was taken because channel orientation in liposome membranes is random, but DIDS is thought to inhibit chloride channels from only one surface (24). Purified catalase (0.01 mg/ml; Sigma-Aldrich) was added under all experimental conditions in order to inhibit potential H_2O_2-dependent effects on anion channel activity potentially caused by high levels of $\cdot O_2^-$.

Encapsulation of xanthine oxidase in proteoliposomes. Proteoliposomes were prepared as described above, with the exception that lipid films were hydrated with a 12.5-U/ml solution of xanthine oxidase (Sigma-Aldrich) in 20 mM KCl buffer. Following sonication, proteoliposomes were eluted down a Sepharose CL-4B column to remove extravesicular xanthine oxidase. The eluted proteoliposomes were collected, kept on ice, and used on the day of preparation. The proteoliposomes were evaluated at a morphological level by TEM and, for xanthine oxidase encapsulation, by Western blotting. In the latter case, proteoliposomes were incubated in PBS with 50 μg/ml pronase (Roche) or PBS with 50 μg/ml pronase plus Triton X-100 (0.5%) at 37°C for 30 min prior to their resolution by sodium dodecyl sulfate-polyacrylamide gel electrophoresis (SDS-PAGE) and Western blotting using an anti-bovine xanthine oxidase antibody (Abcam). Furthermore, proteoliposomes were incubated with xanthine (Sigma-Aldrich) before and after sonication, and the rate of $\cdot O_2^-$ production was measured using the lucigenin-based chemiluminescence assay described above.

Xanthine transport across proteoliposome membranes. To assess xanthine movement across proteoliposome membranes, we incubated vesicles with 500 μM xanthine containing 5 μCi [^{3}H]xanthine (Moravek Biochemicals), in a total volume of 1.0 ml, for 1 h. Aliquots of the proteoliposome suspensions were then taken at different time points and eluted over a Sepharose CL-4B column to remove extravesicular [^{3}H]xanthine. The intravesicular radioactivity was then quantified in a scintillation counter. The counts were expressed as a percentage of the radioactivity of proteoliposomes that were fully hydrated with the xanthine-[^{3}H]xanthine solution used for the uptake assays.

Chemiluminescence assay for $\cdot O_2^-$ transport in proteoliposomes. Xanthine oxidase-loaded proteoliposomes were incubated with a chemiluminescent probe (5 μM lucigenin, 50 μM luminol, or 50 μM isoluminol) for 10 min in the dark at room temperature prior to the addition of 500 μM xanthine to initiate $\cdot O_2^-$ production. $\cdot O_2^-$-derived chemiluminescence was then measured continuously for 10 min, and the rate was calculated from the linear slope of chemiluminescence. For inhibition studies, purified bovine SOD1 (0.01 mg/ml) and/or DIDS (100 μM) was incubated with the proteoliposomes for 10 min prior to the addition of xanthine and the assessment of $\cdot O_2^-$ production rates. In studies comparing various probes or treatment conditions, the same batch of vesicles was always used to generate equal numbers of samples for every condition within a single experimental run. Independent experiments were replicated at least three times. The amounts of vesicles needed for assays with luminol and isoluminol were approximately fivefold greater than that for lucigenin. In studies comparing lucigenin, luminol, and isoluminol, the amounts of vesicles were adjusted to give similar luminescent ranges so that rates were calculated at similar ranges of sensitivity.

BSA-biotin assay for proteoliposome integrity. To determine the extent to which $\cdot O_2^-$ production might negatively impact proteoliposome membrane integrity, we assessed the extent to which encapsulated BSA-biotin was released from proteoliposomes during $\cdot O_2^-$ flux assays. To this end, proteoliposomes were prepared by encapsulating 12.5 U/ml xanthine oxidase and 5 ng/ml BSA-biotin (Sigma-Aldrich). They were then incubated with 500 μM xanthine for 20 min in the presence or absence of SOD1 (0.01 mg/ml) and/or DIDS (100 μM). For all conditions, the integrity of the proteoliposomes during this 20-min period was determined using an enzyme-linked immunosorbent assay. In brief, Neutravidin-labeled 96-well plates (Pierce) were washed three times with wash buffer (25 mM Tris, 150 mM NaCl [pH 7.2], 0.1% BSA), and 200 μl of proteoliposome aliquots diluted 1,000-fold was added to the wells and incubated for 30 min at room temperature. The proteoliposomes were removed, and the wells were washed three times with wash buffer prior to the addition of anti-BSA antibody (Abcam) for 1 h at room temperature. The wells were washed three times with wash buffer before they were incubated with a horseradish peroxidase (HRP)-conjugated secondary antibody (Jackson Immunoresearch) for 1 h at room temperature. 3,3,5,5-Tetramethylbenzidine (200 μl; Sigma-Aldrich), an HRP substrate, was added to the wells for 10 min, and the reaction was stopped by adding 100 μl of 0.5 M H_2SO_4 to each well. The optical density of the solution in each well was then measured at 450 nm. The addition of Triton X-100 (0.5%) to proteoliposomes prior to performing this assay served as a control for 100% leakage. The relative BSA-biotin leakage in experimental samples was determined as the percentage of that seen in the presence of Triton X-100, and this was termed the leakage index.

NF-κB activation assays in SOD1 knockout fibroblasts. (i) Isolation of PMDFs. Primary mouse dermal fibroblasts (PMDFs) were isolated from SOD1 knockout mice (25) (strain B6; 129S7-*Sod1tm1Leb*/J; stock no. 002972; Jackson Laboratory) or wild-type littermate controls. One-day-old pups were euthanized, and their skins were immediately removed and cleaned with sterile PBS. The limbs and tails were also removed and homogenized, and the resulting tissue lysate was then used for rapid genotyping based on Western blotting for SOD1. Skin from each pup was separately placed dermal-side down onto 0.25% trypsin-EDTA solution in a sterile 35-mm petri dish and floated overnight at 4°C. The following day, the epidermis was peeled away from the dermis, and the dermis was incubated in 0.2% collagenase in Dulbecco's modified Eagle medium for 1 h at 37°C. The dermis was then shaken to release the fibroblasts, and this mixed cell population was pelleted and plated in Dulbecco's modified Eagle medium with 10% fetal bovine serum, 1% penicillin-streptomycin, 2.5 U/ml amphotericin B, and 2 mM L-glutamine (fibroblast medium). Cultures were grown in a 5% humidified CO_2, 37°C incubator.

(ii) Assessment of NF-κB transcriptional activity. NF-κB transcriptional activity was assessed using an NF-κB-inducible luciferase reporter delivered into cells using a recombinant adenoviral vector (Ad.NFκBLuc). Briefly, fibroblasts were prepared as described above, seeded in 12-well plates, and incubated overnight in fibroblast medium. The fibroblasts were then infected with 300 particles/cell of Ad.NFκBLuc virus for 4 h in serum-free fibroblast medium. Following infection, the virus and medium were removed and replaced with fresh fibroblast medium, and cells were grown for an additional 48 h. Luciferin was added to the fibroblasts at a concentration of 60 μg/ml for 5 min, and NF-κB activation was determined by measuring luminescence from the luciferase reporter using a Xenogen IVIS imaging system. This was followed by treatment with 50 ng/ml IL-1β and reassessment of NF-κB activation at several time points up to 8 h. In vitro IκB kinase (IKK) assays were also performed as a measure of IKK activity using a previously described protocol (20). In brief, immunoprecipitated IKK was used to phosphorylate glutathione *S*-transferase (GST)-IκBα, and the extent of phosphorylation was evaluated by autoradiography.

RESULTS

Topology of NADPH-dependent $\cdot O_2^-$ production by IL-1β-stimulated endosomes. As previously reported (20), stimulation of MCF-7 cells with IL-1β led to the induction of NADPH-dependent $\cdot O_2^-$ production in endosomal fractions (fractions 2 and 3) following iodixanol gradient fractionation (Fig. 1A). NADPH-dependent $\cdot O_2^-$ production was abrogated when endosomes were loaded with purified bovine SOD1 (bSOD1) protein at the time of IL-1β stimulation (Fig. 1B). Additionally, the abundance of endogenous human SOD1 (hSOD1) in the endosomal compartment increased following IL-1β stimulation, relative to a general endosomal marker Rab11 (Fig. 1B). Given that the membrane-permeable chemiluminescent probe lucigenin was used to

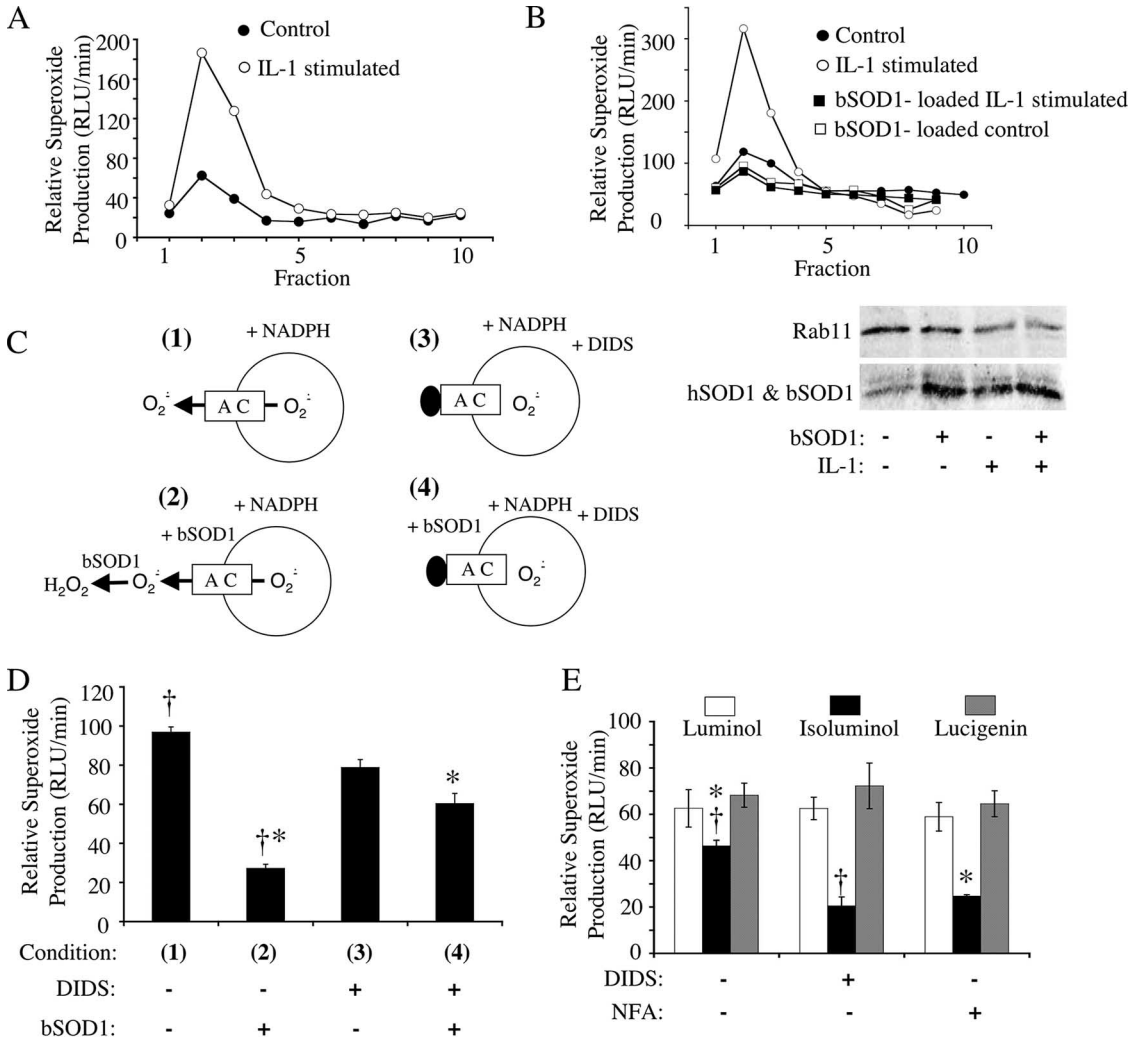

FIG. 1. IL-1β-stimulated endosomes produce NADPH-dependent intravesicular $\cdot O_2^-$ that can permeate endosomal membranes through a DIDS- and NFA-sensitive pathway. MCF-7 cells were stimulated with IL-1β (5 ng/ml) or vehicle for 20 min. The cells were lysed, and PNSs were fractionated on iodixanol gradients. (A) Fractions were evaluated for NADPH-dependent $\cdot O_2^-$ production using a lucigenin-based luminescence assay. (B) MCF-7 cells were treated as described for panel A except that control and IL-1β stimulation were done in the presence or absence of 1 mg/ml SOD1 added to the medium at the time of stimulation. PNSs were fractionated on iodixanol gradients, and Western blotting (lower panel) was performed on the endosomal peak fraction (fraction 2) using antibodies against SOD1 and Rab11 (general endosomal marker). Results of one representative experiment of three are shown in panels A and B. (C) Strategy for assessing NADPH-dependent $\cdot O_2^-$ flux (D) using a lucigenin-based luminescence assay on peak endosomal fraction 2 from IL-1β-stimulated cells. In these studies, SOD1 (0.01 mg/ml) and/or DIDS (100 μM) was added to the outside of isolated endosomes prior to adding NADPH to initiate $\cdot O_2^-$ production. (D) The relative rate of $\cdot O_2^-$ production under the conditions shown in panel C. Results are means and standard errors of the means from three experiments. (E) Comparison of NADPH-dependent $\cdot O_2^-$ production levels by peak endosomal fraction 2 from IL-1β-stimulated cells in the presence of membrane-permeable (lucigenin and luminol) and membrane-impermeable (isoluminol) luminescent probes. Assays were performed in the presence or absence of 100 μM DIDS or NFA. Results are means and standard errors of the means from three experiments. Statistical differences obtained with Student's *t* test ($P < 0.005$) are indicated (*, †). RLU, relative light units.

detect $\cdot O_2^-$, the ability of intraendosomal loading of bSOD1 to quench the $\cdot O_2^-$ signal produced by IL-1β-stimulated endosomes suggests that the majority of $\cdot O_2^-$ is likely produced within the endosome interior and accessible to bSOD1-mediated dismutation.

To investigate whether the intraluminal $\cdot O_2^-$ produced by IL-1β-stimulated endosomes has the ability to move across the endosomal membrane, we performed the above-described experiments in reverse—we exposed IL-1β-stimulated endosomes to purified bSOD1 after fractionation (Fig. 1C). In this manner, we assessed the ability of extravesicular bSOD1 to quench NADPH-dependent $\cdot O_2^-$ production by lucigenin. If extravesicular SOD1 could quench the lucigenin signal under these conditions, it would suggest that a fraction of $\cdot O_2^-$ moves out of IL-1β-stimulated endosomes. Indeed, like endosome-loaded bSOD1, extravesicular bSOD1 effectively quenched the $\cdot O_2^-$ signal by ~75% (Fig. 1D). These findings suggested two possibilities: isolated endosomes did not remain intact in our assays, or $\cdot O_2^-$ was generated within the endosome but rapidly transported out. We reasoned that if a facilitated $\cdot O_2^-$ transport pathway exists in endosomal membranes, such a pathway likely involves an anion channel. In support of this notion, previous studies reported the existence of

a DIDS-sensitive anion channel in mitochondrial and plasma membranes, which are permeable to $\cdot O_2^-$ (11, 13). Thus, we sought to differentiate between the potential mechanisms of the observed $\cdot O_2^-$ quenching by testing whether extravesicular bSOD1 could be rescued by inhibiting the exit of $\cdot O_2^-$ through a putative DIDS-sensitive anion channel (Fig. 1C). Indeed, the addition of DIDS significantly reduced the quenching effect of extravesicular SOD1 to ~23%, compared to ~75% in the absence of DIDS (Fig. 1D). These studies provided strong, albeit indirect, evidence for the ability of $\cdot O_2^-$ to permeate endosomal membranes.

Since membranes are permeable to lucigenin, this probe could not directly distinguish between $\cdot O_2^-$ accumulation inside and outside isolated endosomes. To accomplish this, we developed an alternative approach involving two related luminescent probes for $\cdot O_2^-$ with selective membrane permeability (membrane-permeable luminol and membrane-impermeable isoluminol) (21). As in the case of membrane-permeable lucigenin, detection of NADPH-dependent $\cdot O_2^-$ in isolated IL-1β-stimulated endosomes with membrane-permeable luminol was insensitive to DIDS as well as a second general anion channel blocker, NFA (Fig. 1E). In contrast, detection of $\cdot O_2^-$ in the same endosomal populations with membrane-impermeable isoluminol was inhibited by both DIDS (60% of the level seen in untreated endosomes) and NFA (50% of the level seen in untreated endosomes) (Fig. 1E). These findings provide direct evidence that $\cdot O_2^-$ permeates endosomal membranes through a DIDS/NFA-sensitive pathway. Additionally, the luminol studies demonstrated that the block in anion channel activity does not indirectly inhibit NADPH-dependent $\cdot O_2^-$ production by the Nox complex.

Of interest in these studies was the observation that isoluminol detected 74% of NADPH-dependent $\cdot O_2^-$ in comparison to luminol (Fig. 1E). Given that isoluminol and luminol have similar sensitivities for detecting $\cdot O_2^-$ at the concentration used, these findings suggest that, once generated in the interior of endosomes, $\cdot O_2^-$ exits very rapidly, before it can spontaneous dismutate. This hypothesis is also supported by the extravesicular bSOD1-quenching studies in which membrane-permeable lucigenin was used as a probe (Fig. 1D). In both cases, approximately 70 to 75% of $\cdot O_2^-$ generated in response to NADPH appeared to exit the endosome rapidly. The fact that either DIDS or NFA could block this transport suggests that $\cdot O_2^-$ movement occurs by a facilitated process rather than being a consequence of nonspecific endomembrane leakage.

Inhibition of endosomal anion channels by DIDS enhances ROS accumulation within endosomes. Our data thus far suggested that DIDS-sensitive anion channels in the endosomal compartment are capable of mediating the efflux of $\cdot O_2^-$ from the endosome following IL-1β stimulation. We hypothesized that this pathway may also be active in intact cells and sought supporting data by examining the effects of DIDS treatment on the ability of intact IL-1β-stimulated cells to inhibit $\cdot O_2^-$ efflux out of the endosomal compartment. To this end, we used a recently described method capable of fluorescently detecting $\cdot O_2^-$-dependent ROS accumulation within the endosomal compartment of intact cells. This approach involved endosomal loading with the membrane-impermeable fluorochrome H_2HFF (Oxyburst green)-BSA (20). This previous study demonstrated that IL-1β-stimulated H_2HFF-BSA fluorescence in the endosomal compartment is inhibited by endosomal loading with purified bSOD1 but not catalase, suggesting that redox activation of the dye is caused by either $\cdot O_2^-$ itself or a non-H_2O_2 intermediate product of $\cdot O_2^-$. H_2HFF-BSA fluorescence in the endosomal compartment was significantly enhanced by IL-1β stimulation (Fig. 2A). Treatment of cells

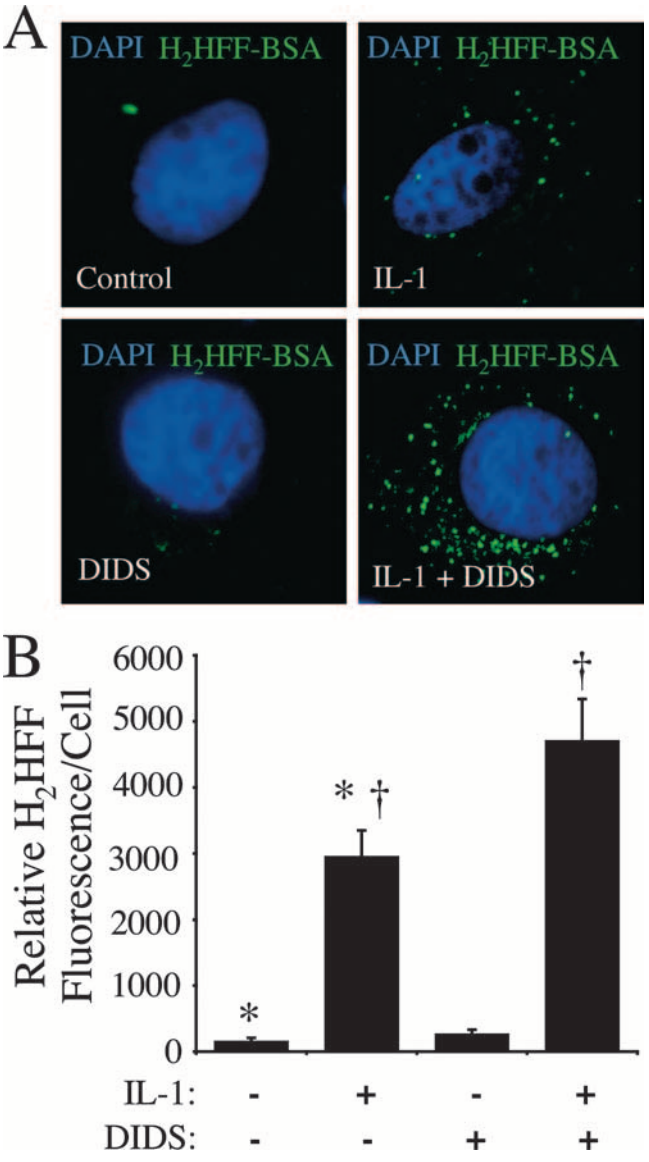

FIG. 2. DIDS treatment of MCF-7 cells at the time of IL-1β stimulation increases intraendosomal $\cdot O_2^-$. Endosomal $\cdot O_2^-$ production by MCF-7 cells was detected using H_2HFF-BSA (50 μg/ml) loaded into the endosomal compartment following stimulation with IL-1β (50 ng/ml) for 20 min. (A) Representative fluorescent images of MCF-7 cells stained with H_2HFF and DAPI following the treatments indicated in the lower-left corner of each panel. DIDS (500 μM) was added 10 min prior to IL-1β stimulation. The cells were fixed in 4% paraformaldehyde 20 min after IL-1β treatment and stained with DAPI (blue) for localization of the nucleus. The green fluorescence represents oxidized H_2HFF resulting from $\cdot O_2^-$ production. Images were taken with a 63× objective. (B) Quantification of H_2HFF fluorescence for the conditions shown in panel A. The relative levels of fluorescence for the treatment groups ($n = 5$) were compared using one-way analysis of variance followed by the Bonferroni posttest (†, $P < 0.05$).

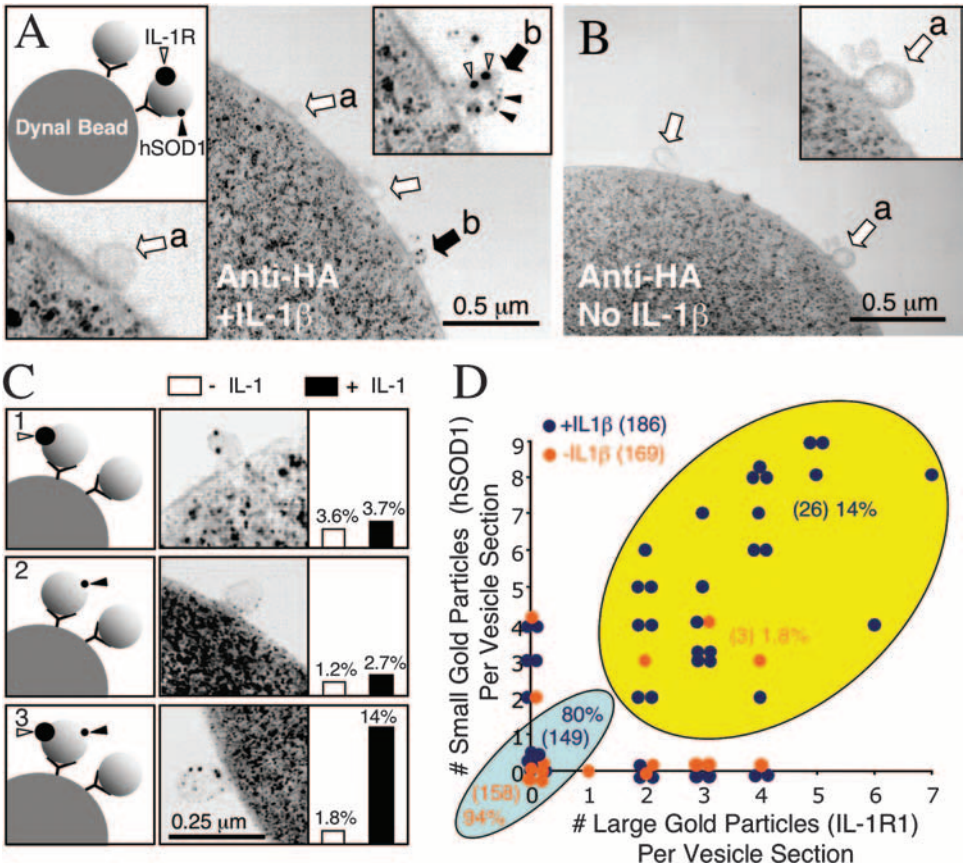

FIG. 3. IL-1β induces SOD1 recruitment to Rab5-expressing early endosomes containing the IL-1 receptor. MCF-7 cells were transfected with HA-Rab5 or green fluorescent protein expression plasmids and stimulated with IL-1β for 20 min. Iodixanol-purified vesicular peak fractions were used for immunoaffinity isolation of HA-Rab5-associated endosomes on anti-HA Dynabeads. Dynabeads were then fixed and immunostained for SOD1 (0.8-nm gold) or IL-1R1 (10-nm gold), postfixed, embedded in Epon, and sectioned for analysis by TEM. Electron micrographs of the Dynabead surface from IL-1β-stimulated (A) and unstimulated (B) HA-immunoabsorbed endosomes (open arrows mark unlabeled endosomes; solid arrows mark endosomes colabeled with both small and large gold particles; open arrowheads mark 10-nm gold [IL-1R1]; solid arrowheads mark 0.8-nm gold [SOD1]). Insets in each panel show enlarged views of vesicles without (a) or with (b) gold label. Cells transfected with green fluorescent protein plasmids demonstrated no significant endosomal binding to anti-HA-beads (data not shown). (C) Examples of labeling patterns that were quantified, along with their relative abundance among the endosomes bound to beads in IL-1β-treated and untreated samples. (D) Changes in the distribution of HA-Rab5-absorbed endosomes positive for both SOD1 and IL-1R1 in the IL-1β-stimulated (dark blue) and unstimulated (orange) samples. Total endosomes quantified for both conditions are given in brackets. Additionally, the total numbers of endosomes in each of the two major categories (light blue, not labeled; yellow, double labeled) are given in parentheses, along with their percentages of the total endosomal population.

with DIDS at the time of IL-1β stimulation significantly enhanced endosomal H_2HFF fluorescence by 60% ($P < 0.05$, analysis of variance and Bonferroni posttest), as one might expect if $\cdot O_2^-$ efflux from the endosome was blocked. These findings provide in vitro support for the existence of endosomal $\cdot O_2^-$ efflux pathways. To control for potential nonspecific effects of DIDS on the uptake of H_2HFF-BSA, we also performed standard endocytic assays with biotin-BSA. These studies demonstrated that DIDS had no effect on the uptake of biotin-BSA into the endosomal compartment during the time course of these assays (data not shown). Therefore, enhanced H_2HFF fluorescence observed following IL-1β stimulation in the presence of DIDS was not the result of enhanced DIDS-mediated endocytosis of H_2HFF-BSA.

SOD1 is actively recruited to IL-1R-containing endosomes following IL-1β stimulation. One of the more intriguing features of ligand-stimulated, redox-active endosomes is the recruitment of endogenous cellular hSOD1 to their surface (Fig. 1B) (20). Together with the above-described studies demonstrating NADPH-dependent $\cdot O_2^-$ efflux from IL-1β-activated endosomes, these findings suggest that endogenous hSOD1 might play a critical role in generating H_2O_2 at the endosomal surface, where ligand-activated receptors reside. Although hSOD1 recruitment to IL-1β-activated endosomes suggests this might indeed occur on endosomes that harbor the IL-1R complex, it does not formally prove that the ligand-activated receptor and hSOD1 are recruited to the same endosome. Such information would support a functional link between IL-1R activation and hSOD1-mediated dismutation of $\cdot O_2^-$ on the endosome surface. We thus directly evaluated the effect of IL-1β stimulation on the colocalization of IL-1R1 and hSOD1, using immuno-electron microscopy examination of HA-Rab5 immuno-absorbed early endosomes.

As shown in Fig. 3, colocalization of IL-1R1 (10-nm gold)

TABLE 1. Classification of IL-1R1 and/or hSOD1 localization to Rab5 early endosomes[a]

Condition	No. (%) of endosomes observed			
	No label	IL-1R1 positive	SOD1 positive	IL-1R1 + SOD1 positive
Unstimulated	158 (93.5)	6 (3.6)	2 (1.2)	3 (1.8)
IL-1 stimulated	149 (80)	7 (3.7)	5 (2.7)	26 (14.0)

[a] Quantification of large gold (IL-1R1)- and small gold (hSOD1)-positive HA-Rab5 affinity-purified endosomes harvested from MCF-7 cells treated with or without IL-1. Data were extracted from Fig. 3D and are total numbers of endosomes observed for each classification (regardless of the number of gold particles).

and hSOD1 (0.8-nm gold) within the same Rab5 early endosome increased significantly (from 1.8% to 14%; Pearson's chi-square test, $P < 0.0003$) following stimulation with IL-1β, whereas the percentage of vesicles that harbored either IL-1R1 or hSOD1 alone did not change significantly (Fig. 3C and Table 1). The majority of endosomes contained neither IL-1R1 nor hSOD1, regardless of whether cells were stimulated by IL-1β (93% in absence versus 80% in presence). This is not surprising given that the Rab5 early endosome compartment is continuously active in cells even in the absence of cytokine stimulation. Interestingly, we saw a strong correlation in the abundance of gold particles labeling hSOD1 and IL-1R1 within a given vesicle following IL-1β stimulation (Pearson correlation test, $P < 0.0025$; Spearman correlation test, $P < 0.0014$), suggesting that the number of IL-1 receptors recruited into a single endosome influences the number of hSOD1 molecules recruited to the same vesicle. However, the absolute ratio of hSOD1 to IL-1R in a given vesicle could not be determined, since the antibodies used likely differ in their binding efficiencies. Our findings demonstrating corecruitment of hSOD1 and IL-1R1 to the same IL-1β-activated endosomes suggest that hSOD1 is in the correct location to influence H_2O_2 production at the endosomal surface, potentially dismutating $\cdot O_2^-$ as it exits.

$\cdot O_2^-$ can compete for Cl^- movement into endomembrane proteoliposomes. The ability of DIDS and NFA to block NADPH-dependent $\cdot O_2^-$ efflux from intact IL-1β-activated endosomes suggests that the pathway for $\cdot O_2^-$ movement may involve an anion channel. Cl^- channels are highly abundant within endosomal membranes and are thus prime candidates for facilitated $\cdot O_2^-$ transport. Membrane depolarization in the phagosome, due to NADPH oxidase electron transfer, requires the influx of counterions (H^+ or K^+) to prevent shutdown of the NADPH oxidase complex (6). Hence, the use of anion channel blockers to study NADPH-dependent $\cdot O_2^-$ production in intact endosomes could potentially be complicated by interference with charge compensation pathways required to keep the Nox complex active. Although our studies detecting NADPH-dependent $\cdot O_2^-$ in the presence of luminol suggest that Nox activity is not reduced in the presence of DIDS or NFA, we sought to confirm that endosomes harbor anion channels capable of passing $\cdot O_2^-$. To this end, we used an X/XO reconstitution system that is not influenced by NADPH oxidase activity.

We assessed whether X/XO-derived $\cdot O_2^-$ could compete for Cl^- transport across endomembrane proteoliposomes using an electrogenic flux assay described by Garty et al. (7) and modified by Goldberg and Miller (9). In this assay, a large Cl^- gradient is formed across Cl^--loaded proteoliposomes by encapsulating highly concentrated KCl inside the vesicles and replacing external Cl^- with the impermeable glutamate anion (potassium glutamate). The movement of Cl^- down this chemical gradient, in the case of proteoliposomes that contain Cl^- channels, creates a high membrane potential (positive inside) within the proteoliposomes. $^{36}Cl^-$ added externally moves down this gradient to accumulate inside the proteoliposomes, a process that was quantified following rapid gel filtration to remove extravesicular $^{36}Cl^-$. This protocol was then combined with DIDS- or X/XO-derived $\cdot O_2^-$ to inhibit or compete for $^{36}Cl^-$ movement into liposomes, respectively (Fig. 4A). Treatment with DIDS significantly inhibited $^{36}Cl^-$ uptake into the liposomes in this scenario, demonstrating that Cl^- channels do indeed exist within endomembrane-generated proteoliposomes and that these endomembranes are anion selective (Fig. 4B).

In this electrogenic flux assay, the uptake of external permeant anions is predicted to reduce the proteoliposome membrane potential and thus to inhibit the concentrative uptake of $^{36}Cl^-$. This effect was observed following X/XO-mediated generation of $\cdot O_2^-$ outside proteoliposomes (Fig. 4B); $^{36}Cl^-$ accumulation within liposomes was reduced by 50% in the presence of $\cdot O_2^-$. To control for potential nonspecific redox-dependent inactivation of anion or activation of cation channels by either $\cdot O_2^-$ or its product H_2O_2, we performed all experiments in the presence of catalase. An additional control for $\cdot O_2^-$-dependent changes in anion or cation channel activity included proteoliposome pretreatment with X/XO for 20 min in the presence of catalase, followed by the addition of SOD1 for 10 min to remove all $\cdot O_2^-$. $^{36}Cl^-$ uptake was then assessed for 20 min as in the case of other test conditions, followed by separation on a Dowex-1 column. As shown in Fig. 4B, pre-exposure of proteoliposomes to $\cdot O_2^-$ in this control assay did not alter $^{36}Cl^-$ uptake into vesicles compared to control proteoliposomes that had never been exposed to X/XO-derived $\cdot O_2^-$. These findings provide strong evidence that reduced concentrative uptake of $^{36}Cl^-$ in the presence of $\cdot O_2^-$ was due to a reduction in membrane potential resulting from $\cdot O_2^-$ transport rather than to redox-dependent modification of anion or cation channels.

Direct assessment of $\cdot O_2^-$ efflux from X/XO encapsulated in endomembrane proteoliposomes. To directly assess $\cdot O_2^-$ efflux in endomembrane proteoliposomes, we used an X/XO system to develop a liposome model system that produces $\cdot O_2^-$ inside liposomes. Xanthine oxidase was encapsulated into endosomal proteoliposomes by hydrating a proteolipid film with a xanthine oxidase solution and subsequently removing extravesicular XO by size exclusion Sepharose CL-4B chromatography. The liposomes generated in this manner ranged in size from 100 to 500 nm (Fig. 5A). To conclusively demonstrate that xanthine oxidase was completely encapsulated within liposomes, we treated fractionated xanthine oxidase-loaded proteoliposomes with pronase before or after lysis with Triton X-100 and analyzed them by SDS-PAGE and Western blotting for xanthine oxidase (Fig. 5B). Results from this experiment demonstrated that xanthine oxidase was indeed en-

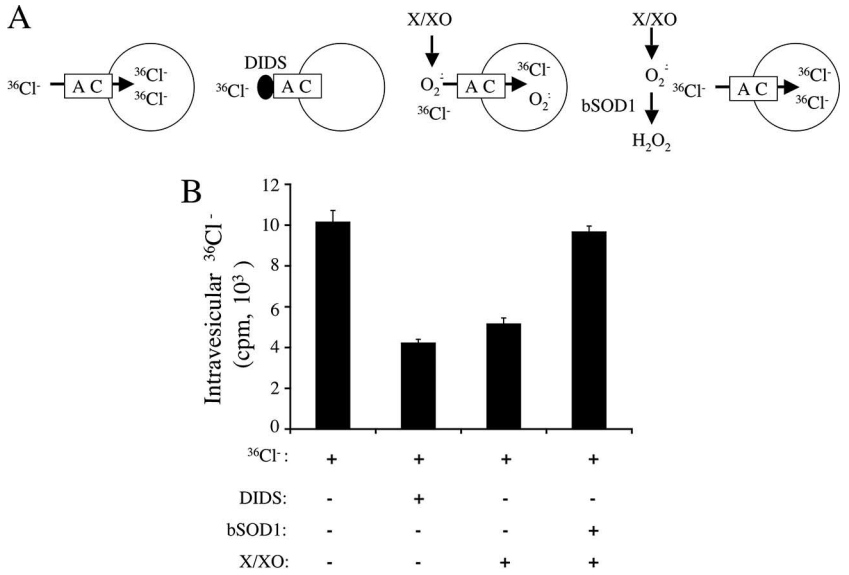

FIG. 4. $\cdot O_2^-$ can compete for Cl^- uptake into endomembrane-reconstituted proteoliposomes through a DIDS-sensitive anion channel. MCF-7 cells were treated with IL-1β (5 ng/ml), and peak endosomal fractions were isolated on iodixanol gradients. Endomembranes were concentrated from the peak vesicular fractions by centrifugation at 100,000 × *g* for 2 h. The membranes and associated proteins were then reconstituted into liposomes with an intraluminal KCl concentration of 150 mM. This was followed by gel filtration exchange of extraluminal KCl with Cl^--free potassium glutamate buffer (150 mM potassium glutamate). (A) Cl^- transport was initiated by adding external ^{36}Cl to the vesicles in the presence or absence of 100 μM DIDS or X/XO-generated $\cdot O_2^-$. After a 20-min incubation period, the extraliposomal ^{36}Cl was removed by passing proteoliposomes over a Dowex-1 anion-exchange column, and the liposome-associated radioactivity was determined. (B) Quantification of ^{36}Cl uptake into proteoliposomes using the parameters described for panel A (values are means and standard errors of the means; $n = 3$). For the reaction with SOD1, $\cdot O_2^-$ was removed following the 20-min exposure to X/XO by adding purified bovine SOD1 (0.01 mg/ml for 10 min). The assessment of ^{36}Cl uptake into proteoliposomes followed for 20 min. This treatment condition controlled for nonspecific inactivation of anion channels by $\cdot O_2^-$.

capsulated inside the liposomes and that it was hence protected from pronase digestion only in the absence of Triton X-100.

A second variable that had to be considered in this system was the rate of diffusion of xanthine across proteoliposome membranes, an event required for the production of $\cdot O_2^-$ by encapsulated xanthine oxidase. The results of experiments evaluating [^{3}H]xanthine diffusion into proteoliposomes following Sepharose CL-4B chromatography are shown in Fig. 5C and demonstrated that xanthine diffusion into proteoliposomes was linear for the first 40 min. When xanthine oxidase-loaded proteoliposomes were used for the $\cdot O_2^-$ generation assays and lucigenin was used as the probe, the addition of xanthine also led to a near-linear rate of $\cdot O_2^-$ production between 5 and 20 min (Fig. 5D). Lysis of proteoliposomes by sonication significantly enhanced the production of $\cdot O_2^-$ 12-fold during the first 20 min of the reaction, as would be expected if the xanthine oxidase was restricted to the liposome interior and production was limited by the diffusion of xanthine across the lipid bilayer (Fig. 5D).

We next sought to evaluate $\cdot O_2^-$ movement out of xanthine oxidase-loaded proteoliposomes. We used two approaches to accomplish this. In the first, we used an extravesicular SOD1 quenching assay with and without DIDS to block potential permeability pathways for $\cdot O_2^-$ movement out of proteoliposomes. Following the addition of xanthine to xanthine oxidase-loaded proteoliposomes, lucigenin-based detection of $\cdot O_2^-$ demonstrated a linear rate of production that was unaltered by the addition of DIDS (Fig. 6A and B), as one might expect, since lucigenin is membrane permeable. These rates of $\cdot O_2^-$ production were compared in the presence of bSOD1 with or without DIDS (Fig. 6A and B). In the presence of extravesicular bSOD1 (without DIDS), the rate of $\cdot O_2^-$ detection was significantly reduced (76%, $P < 0.005$), supporting the notion that $\cdot O_2^-$ moves out of the proteoliposome following its production. However, when bSOD1 was added externally to the vesicles in the presence of DIDS, the quenching of $\cdot O_2^-$ chemiluminescence by bSOD1 was significantly reduced to 30% ($P < 0.002$). Given that DIDS treatment alone did not alter $\cdot O_2^-$ chemiluminescence in the absence of bSOD1 (Fig. 6A and B), these findings suggest that DIDS inhibits a pathway for $\cdot O_2^-$ movement out of the proteoliposome.

Using an alterative approach that takes advantage of chemiluminescent probes with selective membrane permeabilities (luminol is membrane permeable and isoluminol is membrane impermeable), we next sought to directly evaluate the topology of $\cdot O_2^-$ production and release from xanthine oxidase-loaded liposomes (protein free) or proteoliposomes (Fig. 6C and D). Xanthine oxidase-loaded liposomes generated in the absence of endomembrane proteins served as a control for the selectivity of the two chemiluminescent probes to detect intravesicular $\cdot O_2^-$ production in the absence of potential protein permeability pathways. As shown in Fig. 6C and D, liposomes prepared without endomembrane proteins gave a significantly lower luminescent $\cdot O_2^-$ signal with isoluminol than with luminol, consistent with the known lower membrane permeability of isoluminol. In contrast, in the case of liposomes prepared with endomembrane proteins, no significant difference in lu-

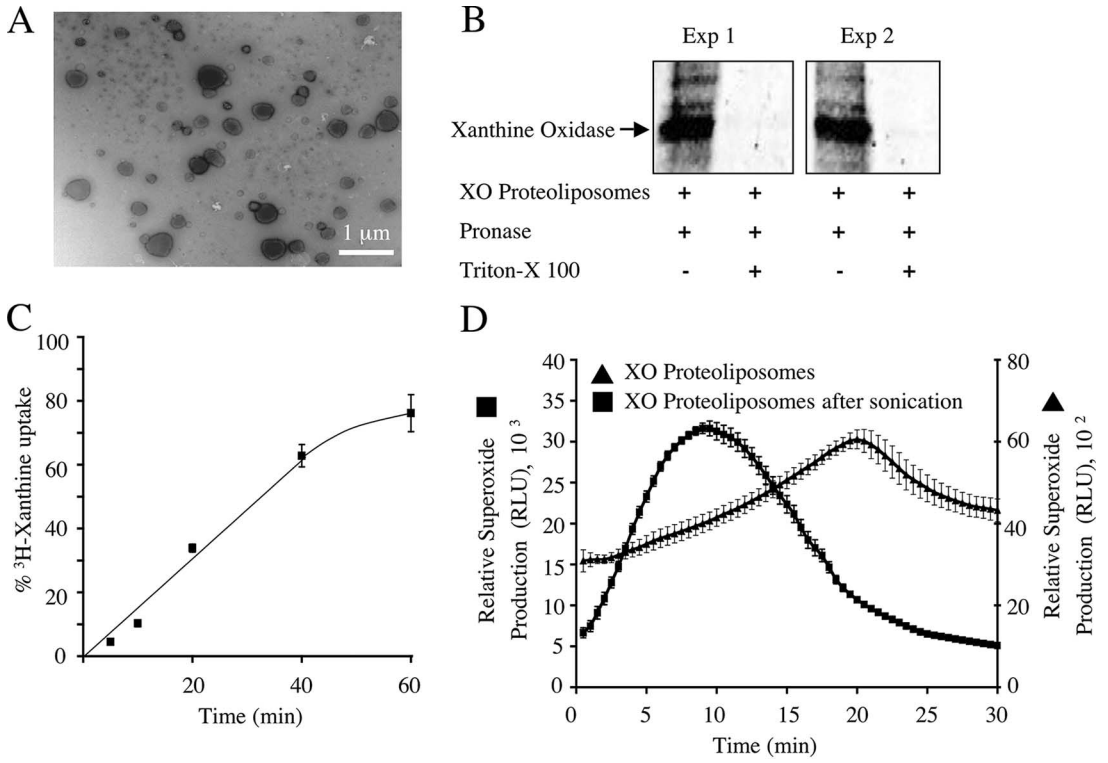

FIG. 5. Proteoliposome model for generating intraluminal $\cdot O_2^-$ anions. MCF-7 cells were treated with IL-1β (5 ng/ml), and peak endosomal fractions were concentrated by centrifugation at 100,000 × *g* for 2 h. Reconstituted proteoliposomes were generated with encapsulated xanthine oxidase. (A) Electron micrograph of xanthine oxidase-loaded proteoliposome. (B) To evaluate encapsulation of xanthine oxidase, the proteoliposomes were incubated in PBS with pronase or in PBS with pronase plus Triton X-100 (0.5%) at 37°C for 30 min. The samples were then separated by SDS-PAGE and analyzed by Western blotting using an anti-xanthine oxidase antibody. (C) The ability of xanthine to enter the proteoliposomes was investigated by incubating the vesicles with [^{3}H]xanthine. Xanthine taken up by proteoliposomes was separated from free xanthine by column chromatography, and the radioactivity associated with the vesicles was measured (values are means and standard errors; n = 3). The time-dependent accumulation of [^{3}H]xanthine within proteoliposomes is expressed as a percentage of maximal loading, as determined by direct encapsulation of [^{3}H]xanthine into proteoliposomes at the time of their synthesis. (D) The ability of xanthine oxidase-loaded proteoliposomes to generate $\cdot O_2^-$ in the presence of extravesicular xanthine was determined using lucigenin-based chemiluminescence. Both native and sonicated proteoliposomes were evaluated for $\cdot O_2^-$ production (values are means and standard errors of the means; n = 3). RLU, relative light units.

minescent $\cdot O_2^-$ signal was observed when the two probes were used. This finding demonstrates that endomembrane proteins can facilitate the movement of $\cdot O_2^-$ out of proteoliposomes.

One potential issue for the liposome and proteoliposome experiments was the extent to which destabilization of the liposomal membrane contributes to passive movement of $\cdot O_2^-$ out of proteoliposomes and protein-free liposomes. Indeed, detection of extravesicular $\cdot O_2^-$ in liposomes by isoluminol suggests that this may occur. To quantify the magnitude of this limitation in this system, we performed studies with BSA-biotin encapsulated in liposomes and proteoliposomes. The extent to which vesicle rupture occurred in these two settings (the leakage index) was evaluated by enzyme-linked immunosorbent assay capture of extravesicular BSA-biotin. As shown in Fig. 7A, incubation of xanthine oxidase-loaded liposomes with or without the xanthine led to an approximately 20% accumulation of extravesicular BSA-biotin relative to that in samples that had been treated with Triton X-100 to intentionally lyse vesicles. These findings demonstrate an approximately 20% background level of vesicle rupture in this assay; nevertheless, destabilization of the liposomes was not promoted by $\cdot O_2^-$ generation. Proteoliposomes appeared to be slightly less stable, with BSA-biotin escape at ~30% under the tested treatment conditions (Fig. 7B). The background leakage of 20 to 30% helps to explain why a low-level $\cdot O_2^-$ signal was detected by isoluminol in X/XO-loaded liposomes (Fig. 6D) and why only 75% of the lucigenin-detected $\cdot O_2^-$ signal was recovered in proteoliposomes treated with DIDS/bSOD1 (Fig. 6B). Hence, if one corrects for leakage in these assays, our results with respect to DIDS-sensitive $\cdot O_2^-$ efflux become even more significant.

SOD1 is important for NF-κB activation. The facilitated efflux of $\cdot O_2^-$ across endosomal membranes harboring activated IL-1 receptors suggests intriguing possibilities for the generation of ROS-mediated signals at the endosome surface. In this context, Nox-derived H_2O_2 plays a key role in the redox-dependent recruitment of TRAF6 to the IL-1R/MyD88 complex, a step that is required for IKK activation of NF-κB (20). Our finding that IL-1β stimulation promotes the recruitment of endogenous SOD1 to endosomes harboring IL-1R suggests the possibility that SOD1 at the surface of these en-

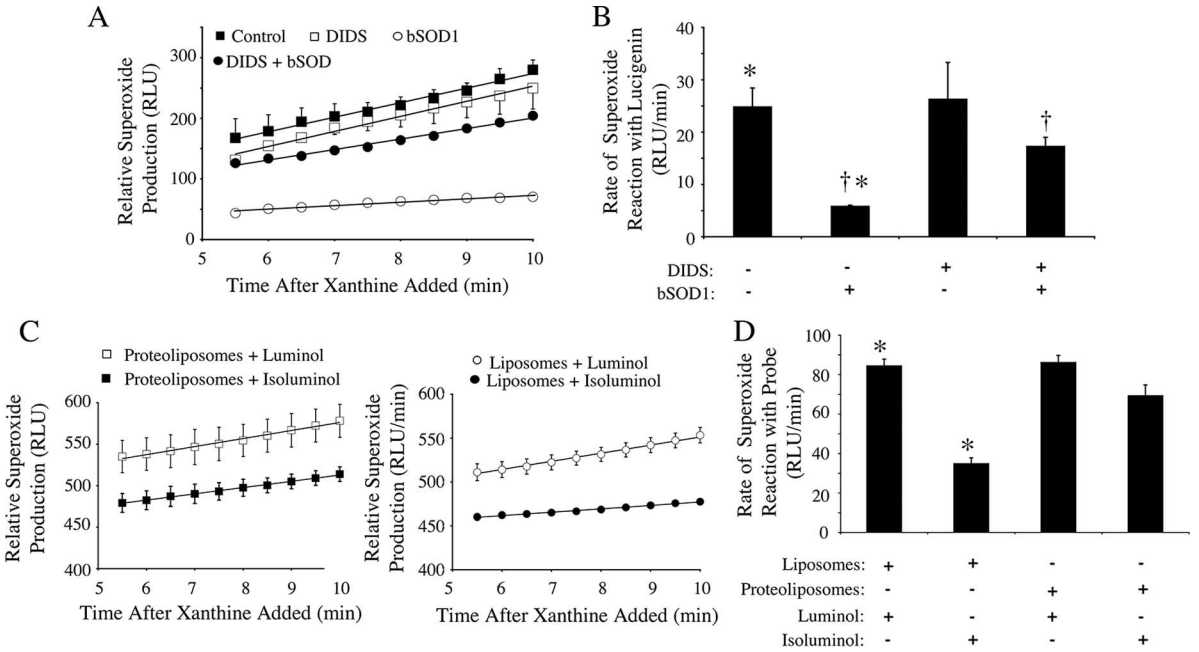

FIG. 6. $\cdot O_2^-$ generation and transport by xanthine oxidase-loaded proteoliposomes and liposomes. Xanthine oxidase-loaded proteoliposomes and liposomes (without membrane proteins) were incubated with xanthine, and $\cdot O_2^-$ anions were detected with the specified luminescent probes at the indicated times after addition of xanthine. (A) Relative $\cdot O_2^-$ production by xanthine oxidase-loaded proteoliposomes was detected using membrane-permeable lucigenin in the presence of 100 μM DIDS, 0.01 mg/ml SOD1, or DIDS and SOD1 (values are means and standard errors of the means; $n = 3$). (B) Relative rates of $\cdot O_2^-$ reaction with lucigenin between 5 and 10 min after addition of xanthine under the various conditions used for panel A (values are means and standard errors of the means; $n = 3$). (C) Luminol (membrane permeable) and isoluminol (membrane impermeable) chemiluminescence was used to compare the movement of $\cdot O_2^-$ anions across liposome membranes to that across proteoliposomes (values are means and standard errors of the means; $n = 3$). (D) The relative rates of $\cdot O_2^-$ reaction with luminol or isoluminol in liposomes or proteoliposomes were quantitated at 5 to 10 min after addition of xanthine. Statistical differences obtained with Student's t test ($P < 0.01$) are indicated (*, †). RLU, relative light units.

dosomes may function in the signaling process. In this regard, we hypothesized that SOD1 at the surface of redox-active endosomes may serve to locally dismutate $\cdot O_2^-$ that crosses endosomal membranes, hence providing a localized source of H_2O_2 to facilitate IKK complex activation by IL-1R. If, indeed, SOD1 is critical for this process, one would predict that NF-κB activation following IL-1β stimulation would be significantly blunted in the absence of SOD1.

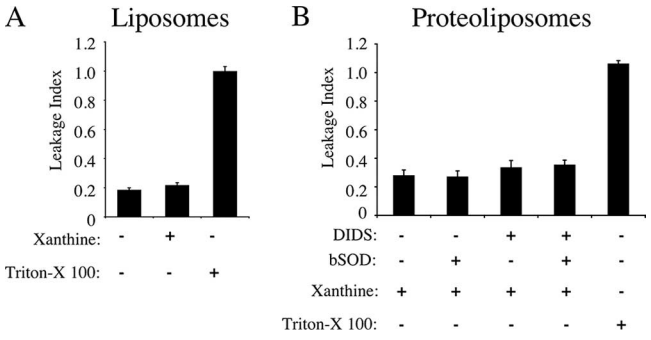

FIG. 7. Integrity of xanthine oxidase-loaded proteoliposomes following $\cdot O_2^-$ production. Liposomes (A) and proteoliposomes (B) were loaded with xanthine oxidase and biotin-BSA and incubated with xanthine for 15 min in the presence of 100 μM DIDS, 0.01 mg/ml SOD1, or DIDS and SOD1. At the end of the incubation, proteoliposomes and liposomes were transferred to Reacti-bind Neutravidin-coated plates to remove extravesicular biotin-BSA. The plates were then incubated with anti-BSA antibody followed by an HRP-conjugated secondary antibody. The HRP substrate 3,3,5,5-tetramethylbenzidine was used to detect HRP activity at 450 nm after addition of 0.5 M H_2SO_4. Values for extravesicular biotin-BSA (leakage index) are expressed as a percentage of the value obtained from samples lysed with 0.5% Triton X-100, a control that represents 100% lysis (values are means and standard errors; $n = 3$).

To investigate the importance of SOD1 in IL-1β-mediated activation of NF-κB, we compared the abilities of wild-type and mSOD1-deficient PMDFs to activate NF-κB following IL-1β stimulation. PMDFs were infected with an NF-κB-responsive luciferase reporter adenoviral vector and evaluated for luciferase expression prior to and following IL-1β stimulation by biophotonic imaging using a Xenogen IVIS imaging system. The results are shown in Fig. 8. In the absence of IL-1β stimulation, the baseline level of NF-κB activation in mSOD1-deficient cells was approximately 2.7-fold lower than that in their wild-type counterparts (Fig. 8C, 0-h and 1-h time points). Moreover, IL-1β stimulation in these cells led to only a marginal increase in NF-κB transcriptional activation over an 8-h period, in contrast to the substantial increase that was seen during this time in wild-type cells (Fig. 8C, 2-h time point and beyond). In support of these findings, IKK activation was observed at 30 min after IL-1β stimulation of wild-type cells but not in SOD1-deficient cells (Fig. 8D). These findings demonstrate that cellular SOD1 indeed influences NF-κB transcriptional activation following IL-1β stimulation and support the notion that SOD1-mediated dismutation of $\cdot O_2^-$ at the endosomal surface may be important for establishing local H_2O_2 gradients that are necessary for IL-1R activation.

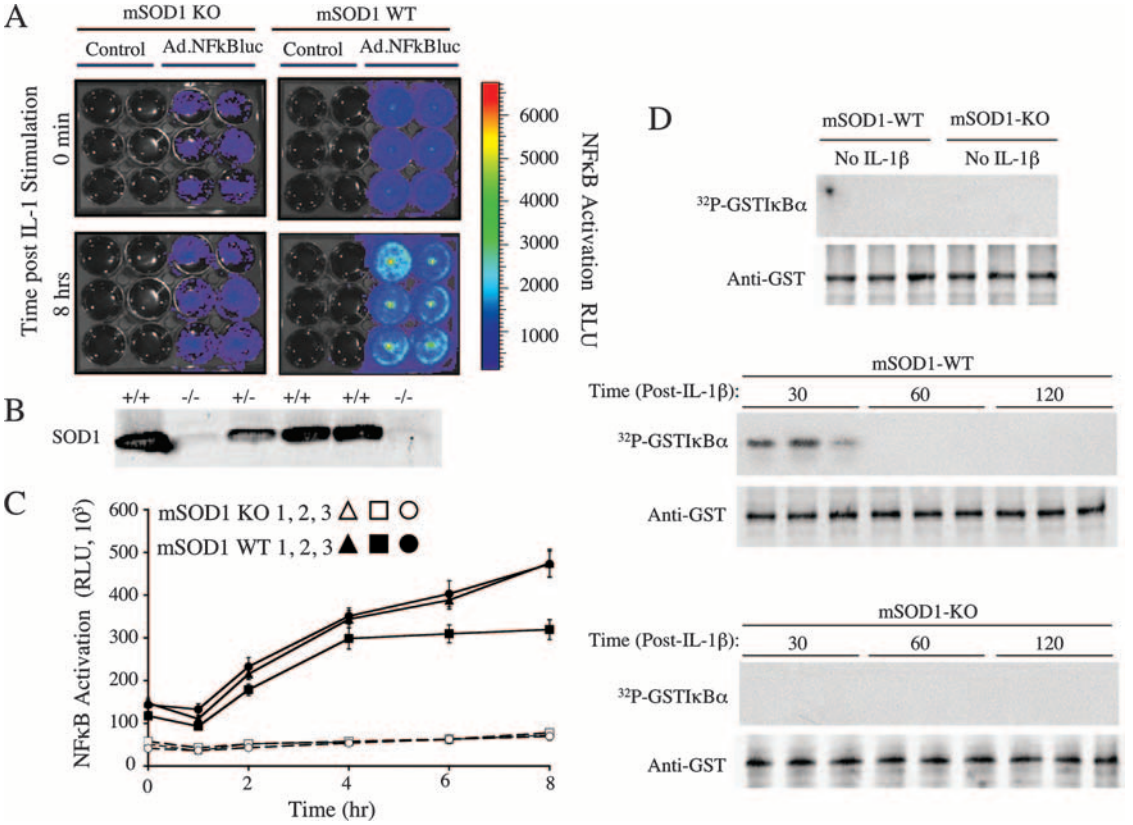

FIG. 8. SOD1 is important for IL-1β-induced NF-κB activation. SOD1 knockout (SOD1-KO) and SOD1 wild-type (SOD1-WT) PMDFs were harvested as described in Materials and Methods and seeded in 12-well plates. Cells were infected with an NF-κB-inducible luciferase reporter carried on a recombinant adenoviral vector (Ad.NFκBLuc; multiplicity of infection, 300). Control wells were not infected. Luciferin (60 μg/ml) was added to the fibroblasts, and luciferase activity was assessed with a Xenogen IVIS imaging system. This was done prior to stimulation with IL-1β (50 ng/ml) and at several time points up to 8 h poststimulation. (A) Detection of NF-κB-inducible luciferase activity by the Xenogen IVIS imaging system. Representative wells are shown for SOD1 knockout and SOD1 wild-type PMDFs at 0 min and 8 h poststimulation. (B) Western blot for SOD1 protein in tissue from a litter of mouse pups used to derive PMDFs. Two of the six shown are knockouts (−/−). (C) Time course for NF-κB transcriptional activity following IL-1β stimulation. Values are luminescence (in relative light units [RLU] per well for each PMDF genotype (means and standard errors of the means; $n = 6$). (D) IKK assays for stimulation with IL-1β (50 ng/ml) at various time points. Samples were resolved by SDS-PAGE and transferred to nitrocellulose prior to autoradiography. Shown are results for three representative samples for each condition, including the control (unstimulated) and 30, 60, and 120 min after IL-1β stimulation. The top panel in each set shows a ^{32}P-labeled GST-IκBα autoradiogram, and the bottom panel is a Western blot of the same filter with anti-GST antibody to control for sample loading.

DISCUSSION

The spatial regulation of Nox activation by cells following receptor activation has become increasingly recognized as a critical component of redox signaling (31). In this context, IL-1 stimulates endosomal production of luminal $\cdot O_2^-$, and its product H_2O_2 is known to be required for the redox-dependent activation of the IL-1R1 complex and hence the ability of this complex to activate IKK and NF-κB (20). Our studies provide further evidence that cellular SOD1 is actively recruited to IL-1R1-bearing redox-active endosomes following ligand stimulation. This feature of SOD1 recruitment to the surface of $\cdot O_2^-$-producing endosomes suggests that $\cdot O_2^-$ dismutation at the endosomal surface may be tightly regulated. The local dismutation of $\cdot O_2^-$ may play a key role in activating H_2O_2-dependent effectors at the endosomal surface or, as recently suggested, may also directly regulate the activity of Rac1-dependent Nox complexes on endosomes (12). However, since lipid membranes are impermeable to $\cdot O_2^-$ (10), such hypotheses do not seem possible without a membrane permeability pathway for $\cdot O_2^-$. Thus, in the present study we sought to assess whether endosomal pathways for $\cdot O_2^-$ movement across the membrane indeed exist, as well as testing whether such control is important in NF-κB activation by IL-1β.

The membrane topology of Nox complexes suggests that $\cdot O_2^-$ is produced either outside the cell (when the relevant Nox resides in the plasma membrane) or in the endosomal lumen (when the Nox complex is in an intracellular compartment) (19). Recent studies by Hawkins et al. have implicated ClC-3 as a plasma membrane-resident $\cdot O_2^-$ channel capable of passing extracellular $\cdot O_2^-$ anions into the cytoplasm of vascular endothelial cells (13). Our data demonstrating that intact endosomes isolated following IL-1β stimulation have DIDS- and NFA-sensitive $\cdot O_2^-$ permeability are consistent with such a mechanism, since both DIDS and NFA are known to inhibit ClC-3. Hawkins et al. suggested that extracellular production of $\cdot O_2^-$ by NADPH oxidases may influence cell signaling through the regulated uptake of $\cdot O_2^-$ at the plasma membrane, and we propose that similar regulation may oc-

cur at the level of the endosome following IL-1β stimulation.

A critical factor in determining if the $\cdot O_2^-$ permeability pathway of IL-1β-induced endosomes involves an anion channel similar to ClC-3 was the demonstration that $\cdot O_2^-$ movement across endosomal membranes is an electrogenic process. Indeed, our studies demonstrating that $\cdot O_2^-$ can compete for Cl^- flux across endosomal membranes suggest that this is the case. Further support for the idea that this pathway involves an anion channel includes the DIDS and NFA sensitivity. Given the fact that the $\cdot O_2^-$ flux observed in native Nox-active endosomes could be reproduced in a analogous system that uses xanthine oxidase-loaded proteoliposomes generated from endosomal membrane proteins, the anion channel that functions as a $\cdot O_2^-$ permeability pathway appears to be functional even in the absence of Nox activation. Whether this unidentified anion channel is specifically recruited to endosomes harboring the ligand-bound IL-1R or is resident in endosomes in the unstimulated state remains to be determined.

Important implications for the identification of a $\cdot O_2^-$ anion channel(s) in endosomes is the potential functional role such a channel might play in redox-dependent cell signaling. Our studies in SOD1-deficient mouse fibroblasts suggest that SOD1 may indeed play a role in local redox-signaling events at the endosome surface, given that IL-1β-mediated IKK and NF-κB induction is significantly reduced in the absence of SOD1. We have also observed that treatment of IL-1β-stimulated MCF-7 cells with DIDS partially inhibits NF-κB (data not shown). This would be expected if DIDS blocked endosomal $\cdot O_2^-$ efflux needed for the localized SOD1-mediated dismutation required for IL-1R activation. It is interesting that SOD1-deficent mice exhibit reduced NF-κB activation in the brain following head injury, while responses in transgenic mice overexpressing SOD1 were similar to those in nontransgenic controls (1). However, transgenic overexpression of SOD1 has also been shown to reduce NF-κB activation following transient focal cerebral ischemia (15). These two seemingly contradictory findings suggest that SOD1 function in redox signaling may be more complex than previously anticipated and that it may be unique to specific types of cellular responses. The localized dismutation of $\cdot O_2^-$ at the endosomal surface by SOD1 is a new potential control mechanism whereby H_2O_2 signals can be spatially regulated at sites of cell signaling.

In summary, we have demonstrated that $\cdot O_2^-$ moves across endosomal membranes during IL-1 signaling and that it does so through a pathway involving an anion channel. These findings provide a framework for understanding why SOD1 is actively recruited to ligand-activated IL-1R-containing endosomes. The localized control of $\cdot O_2^-$ movement across endosomal membranes containing SOD1 provides yet another level of spatial control for ROS metabolism and its influence in cell signaling.

ACKNOWLEDGMENTS

This work was supported by NIDDK (DK067928 and DK51315) (J.F.E.) and core facilities from The Center for Gene Therapy (P30 DK54759).

We gratefully acknowledge Christine Blaumueller for editorial assistance and Fred Oakley for scientific advice in the use of the Xenogen IVIS imaging system. We also thank Randy Nessler in the Gene Therapy Center Morphology Core for technical assistance in immunogold staining.

REFERENCES

1. **Beni, S. M., J. Tsenter, A. G. Alexandrovich, N. Galron-Krool, A. Barzilai, R. Kohen, N. Grigoriadis, C. Simeonidou, and E. Shohami.** 2006. CuZn-SOD deficiency, rather than overexpression, is associated with enhanced recovery and attenuated activation of NF-κB after brain trauma in mice. J. Cereb. Blood Flow Metab. **26:**478–490.
2. **Cadenas, E.** 2004. Mitochondrial free radical production and cell signaling. Mol. Aspects Med. **25:**17–26.
3. **Chance, B., H. Sies, and A. Boveris.** 1979. Hydroperoxide metabolism in mammalian organs. Physiol. Rev. **59:**527–605.
4. **Choi, M. H., I. K. Lee, G. W. Kim, B. U. Kim, Y. H. Han, D. Y. Yu, H. S. Park, K. Y. Kim, J. S. Lee, C. Choi, Y. S. Bae, B. I. Lee, S. G. Rhee, and S. W. Kang.** 2005. Regulation of PDGF signalling and vascular remodelling by peroxiredoxin II. Nature **435:**347–353.
5. **Crapo, J. D., T. Oury, C. Rabouille, J. W. Slot, and L. Y. Chang.** 1992. Copper, zinc superoxide dismutase is primarily a cytosolic protein in human cells. Proc. Natl. Acad. Sci. USA **89:**10405–10409.
6. **Cross, A. R., and A. W. Segal.** 2004. The NADPH oxidase of professional phagocytes–prototype of the NOX electron transport chain systems. Biochim. Biophys. Acta **1657:**1–22.
7. **Garty, H., B. Rudy, and S. J. Karlish.** 1983. A simple and sensitive procedure for measuring isotope fluxes through ion-specific channels in heterogenous populations of membrane vesicles. J. Biol. Chem. **258:**13094–13099.
8. **Georgiou, G.** 2002. How to flip the (redox) switch. Cell **111:**607–610.
9. **Goldberg, A. F., and C. Miller.** 1991. Solubilization and functional reconstitution of a chloride channel from Torpedo californica electroplax. J. Membr. Biol. **124:**199–206.
10. **Gus'kova, R. A., I. I. Ivanov, V. K. Kol'tover, V. V. Akhobadze, and A. B. Rubin.** 1984. Permeability of bilayer lipid membranes for superoxide ($O_2^{-\cdot}$) radicals. Biochim. Biophys. Acta **778:**579–585.
11. **Han, D., F. Antunes, R. Canali, D. Rettori, and E. Cadenas.** 2003. Voltage-dependent anion channels control the release of the superoxide anion from mitochondria to cytosol. J. Biol. Chem. **278:**5557–5563.
12. **Harraz, M. M., J. J. Marden, W. Zhou, Y. Zhang, A. Williams, V. S. Sharov, K. Nelson, M. Luo, H. Paulson, C. Schoneich, and J. F. Engelhardt.** 2008. SOD1 mutations disrupt redox-sensitive Rac regulation of NADPH oxidase in a familial ALS model. J. Clin. Investig. **118:**659–670.
13. **Hawkins, B. J., M. Madesh, C. J. Kirkpatrick, and A. B. Fisher.** 2007. Superoxide flux in endothelial cells via the chloride channel-3 mediates intracellular signaling. Mol. Biol. Cell **18:**2002–2012.
14. **Hordijk, P. L.** 2006. Regulation of NADPH oxidases: the role of Rac proteins. Circ. Res. **98:**453–462.
15. **Huang, C. Y., M. Fujimura, N. Noshita, Y. Y. Chang, and P. H. Chan.** 2001. SOD1 down-regulates NF-κB and c-Myc expression in mice after transient focal cerebral ischemia. J. Cereb. Blood Flow Metab. **21:**163–173.
16. **Ikebuchi, Y., N. Masumoto, K. Tasaka, K. Koike, K. Kasahara, A. Miyake, and O. Tanizawa.** 1991. Superoxide anion increases intracellular pH, intracellular free calcium, and arachidonate release in human amnion cells. J. Biol. Chem. **266:**13233–13237.
17. **Kamata, H., S. Honda, S. Maeda, L. Chang, H. Hirata, and M. Karin.** 2005. Reactive oxygen species promote TNFα-induced death and sustained JNK activation by inhibiting MAP kinase phosphatases. Cell **120:**649–661.
18. **Lambeth, J. D.** 2004. NOX enzymes and the biology of reactive oxygen. Nat. Rev. Immunol. **4:**181–189.
19. **Lassegue, B., and R. E. Clempus.** 2003. Vascular NAD(P)H oxidases: specific features, expression, and regulation. Am. J. Physiol. Regul. Integr. Comp. Physiol. **285:**R277–R297.
20. **Li, Q., M. M. Harraz, W. Zhou, L. N. Zhang, W. Ding, Y. Zhang, T. Eggleston, C. Yeaman, B. Banfi, and J. F. Engelhardt.** 2006. Nox2 and Rac1 regulate H_2O_2-dependent recruitment of TRAF6 to endosomal interleukin-1 receptor complexes. Mol. Cell. Biol. **26:**140–154.
21. **Lundqvist, H., and C. Dahlgren.** 1996. Isoluminol-enhanced chemiluminescence: a sensitive method to study the release of superoxide anion from human neutrophils. Free Radic. Biol. Med. **20:**785–792.
22. **Lynch, R. E., and I. Fridovich.** 1978. Permeation of the erythrocyte stroma by superoxide radical. J. Biol. Chem. **253:**4697–4699.
23. **Mao, G. D., and M. J. Poznansky.** 1992. Electron spin resonance study on the permeability of superoxide radicals in lipid bilayers and biological membranes. FEBS Lett. **305:**233–236.
24. **Matulef, K., and M. Maduke.** 2005. Side-dependent inhibition of a prokaryotic ClC by DIDS. Biophys. J. **89:**1721–1730.
25. **Matzuk, M. M., L. Dionne, Q. Guo, T. R. Kumar, and R. M. Lebovitz.** 1998. Ovarian function in superoxide dismutase 1 and 2 knockout mice. Endocrinology **139:**4008–4011.

26. **Miller, F. J., Jr., M. Filali, G. J. Huss, B. Stanic, A. Chamseddine, T. J. Barna, and F. S. Lamb.** 2007. Cytokine activation of nuclear factor κB in vascular smooth muscle cells requires signaling endosomes containing Nox1 and ClC-3. Circ. Res. **101:**663–671.
27. **Petry, A., T. Djordjevic, M. Weitnauer, T. Kietzmann, J. Hess, and A. Gorlach.** 2006. NOX2 and NOX4 mediate proliferative response in endothelial cells. Antioxid. Redox. Signal. **8:**1473–1484.
28. **Rhee, S. G.** 2006. Cell signaling. H2O2, a necessary evil for cell signaling. Science **312:**1882–1883.
29. **Rhee, S. G., Y. S. Bae, S. R. Lee, and J. Kwon.** 2000. Hydrogen peroxide: a key messenger that modulates protein phosphorylation through cysteine oxidation. Sci. STKE **2000:**PE1.
30. **Salvador, A., J. Sousa, and R. E. Pinto.** 2001. Hydroperoxyl, superoxide and pH gradients in the mitochondrial matrix: a theoretical assessment. Free Radic. Biol. Med. **31:**1208–1215.
31. **Ushio-Fukai, M.** 2006. Localizing NADPH oxidase-derived ROS. Sci. STKE **2006:**re8.
32. **Van Buul, J. D., M. Fernandez-Borja, E. C. Anthony, and P. L. Hordijk.** 2005. Expression and localization of NOX2 and NOX4 in primary human endothelial cells. Antioxid. Redox. Signal. **7:**308–317.